Beam-Aware Topology Optimization in Multi-Hop UAV Networks

Ali Yilmaz Yildirim
Airbus Defence and Space
Chair of Network Architectures and Services
Technical University of Munich
Munich, Germany
ali-yilmaz.yildirim@airbus.com

Fabien Geyer
Airbus Defence and Space
Munich, Germany
fabien.geyer@airbus.com

Georg Carle
Chair of Network Architectures and Services
Technical University of Munich
Munich, Germany
carle@net.in.tum.de

***Abstract*—Unmanned Aerial Vehicles (UAVs) increasingly support mission-critical applications such as disaster recovery and remote sensing. In these airborne networks, overall system performance is often limited by the weakest link, making maximizing the bottleneck link capacity essential for reliable data delivery. This study addresses the challenge of topology optimization by focusing on maximizing the bottleneck link Signal-to-Interference-plus-Noise Ratio (SINR). Beyond simple connectivity, we enforce path redundancy to ensure resilience. We formulate the problem as a Mixed-Integer Non-Linear Programming (MINLP). To ensure computational tractability, the problem is reformulated as a Mixed-Integer Linear Program (MILP). Furthermore, we evaluate metaheuristic algorithms to investigate the trade-offs between solution quality and computational cost. Our findings indicate that while MILP-based topologies achieve higher End-to-End (E2E) capacities with acceptable computational overhead in small-scale networks, metaheuristic frameworks provide near-optimal solutions with significantly lower computational time as network scale increases.**

***Index Terms*—UAVs, Directional Antennas, Mixed-Integer Linear Programming, Grey Wolf Optimizer, Genetic Algorithm, Topology Optimization**

I. Introduction

Unmanned Aerial Vehicle (UAV) utilization has expanded into civilian and military sectors, notably being considered as mobile, low-cost aerial base stations. To improve the spatial efficiency, UAVs have been equipped with high-gain directional antennas operating in Millimeter wave (mmWave) frequencies. Narrow-beam transmissions enabled by directional antennas allow concurrent communication links with reduced inter-link interference.

While UAV network research [1] is expanding, several critical gaps still exist. Most current studies focus on centralized, sub-6 GHz aerial base station deployments, leaving multi-hop airborne networks for mission-critical tasks (e.g., data collection or rescue operations) largely unaddressed. Where such networks are studied, the focus is often restricted to beam tracking for high-mobility nodes [2]. This paper addresses this gap by optimizing the topology of a mmWave-enabled, multi-hop UAV network. We aim to maximize the bottleneck Signal-to-Interference-plus-Noise Ratio (SINR) by determining the optimal set of directional connections. Unlike existing studies that focus on trajectory optimization, we consider scenarios where UAV trajectories are predetermined by the mission profile, such as firefighting, environmental monitoring, or search and rescue. Our study makes the following contributions:

- To ensure fairness among all UAVs, we formulate the objective to maximize the minimum SINR across the network, subject to strict node degree and strongly connected constraints.
- We optimize over a time horizon rather than a single snapshot. This multi-period approach would avoid the frequent reconfigurations.
- We linearize the resulting Mixed Integer Non Linear Programming (MINLP) into a Mixed Integer Linear Programming (MILP) that an exact solver handles in an acceptable time.
- We benchmark Genetic Algorithm (GA) [3] and Grey Wolf Optimizer (GWO) [4] against the exact solution to quantify the trade-off between bottleneck SINR and planning time.

To the best of our knowledge, this study is the first to address topology optimization in UAV ad-hoc networks equipped with directional antennas while considering a time horizon. Our findings provide a framework for constructing networks that optimize multi-hop flows throughout a mission, in which UAV trajectories are predetermined.

The rest of the paper is organized as follows: Section II reviews related work on Topology Control (TC) in different use cases. Section III details the network architecture and the underlying communication parameters. Section IV explains the mathematical problem formulation and the implemented algorithms. Section V explains the simulation scenario, assumptions, and evaluation metrics. Section VI presents a detailed performance analysis and discusses the key findings. Finally, Section VII concludes the paper with a summary of the findings and potential directions for future research.

II. Related Work

TC was first studied in omnidirectional wireless networks, where multi-hop connectivity was established primarily through transmit power adjustment [5]. Subsequent advancements in antenna technology led to the integration of directional antennas into TC frameworks. For instance, Hofmann

979-8-3195-0167-7/26/$31.00 ©2026 IEEE

et al. [6] investigated multi-hop aerial links to extend ground-to-air connectivity in aeronautical ad hoc networks, aiming to maximize the number of aircraft maintaining link quality above a predefined threshold. Although they derived exact solutions using a MILP formulation, computational complexity restricted their evaluation to networks of at most 60 nodes. To address these scalability constraints, Megas et al. [7] proposed a heuristic framework that yields suboptimal solutions within a practical runtime for larger topologies. Newton et al. [8] constructed a Free-Space Optical Communications (FSOC) backbone connecting aircraft and ground gateways, aiming to minimize path hop count while maximizing node degree for enhanced structural robustness. Nevertheless, a fundamental limitation of these static approaches is their reliance on instantaneous snapshot optimizations, which induce frequent topology reconfigurations and incur prohibitive signaling overhead in highly dynamic operational regimes.

The work by [9] closely aligns with our investigation of TC in UAV networks. That study aims to maximize fairness-weighted capacity by jointly optimizing beam directionality, time-slot allocation, and power control. However, their framework does not account for UAV mobility, as the centralized controller assigns resources on a per-second basis. Furthermore, their evaluation is limited to small-scale topologies with up to 16 UAVs and does not assess end-to-end (E2E) throughput metrics for multi-hop communication.

While existing literature has explored TC, the aforementioned gaps remain. To address these gaps for multi-hop UAV Ad-Hoc networks equipped with directional antennas, we implement TC by using different optimization algorithms. Unlike previous studies, which often rely on static snapshots, we formulate and solve the optimization problem over a defined time horizon.

III. System Model

Each UAV is equipped with a set of four mmWave directional antennas, positioned on each face of the platform, with a steering range of 45°. The role of these antennas is to enable data transmission and multi-hop communication across the UAV network. For each node, the total number of active bidirectional connections, referred to as the nodal degree d_i, is kept within constraint as $d_{min} \leq d_i \leq d_{max}$.

A. Network Model

We model UAV Ad-Hoc Network with a directed graph $\mathcal{G} = (\mathcal{V}, \mathcal{E})$, where $\mathcal{V}$ denotes the set of UAVs and $\mathcal{E}$ represents the set of active links. For any UAV pair (i, j) with $(i, j) \in V \times V : i \neq j$, $i \rightarrow j$ vector characterized as $(\theta_{i,j}, \phi_{i,j}, d_{i,j})$ representing the azimuth angle, elevation angle, and distance with respect to UAV body frame. We denote the antenna boresight direction of the transmitter (e_{tx}) directed to receiver (e_{rx}) as azimuth and elevation angles with $[\theta_e, \phi_e]$. By defining the boresight, we can calculate the horizontal deviation angle ($\Delta\theta_{e,j}$) and vertical deviation angle ($\Delta\phi_{e,j}$) between an antenna boresight and any other UAV in the network ($j \in V : i \neq e_{tx}$) as illustrated in Figure 1.

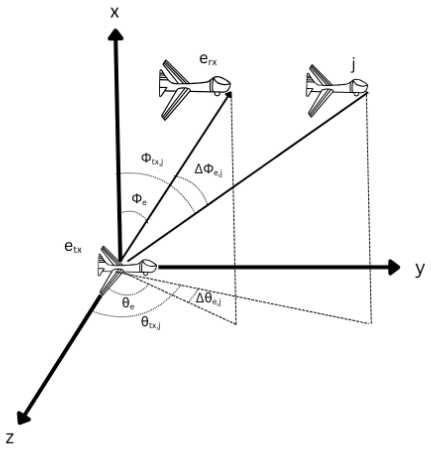


Fig. 1: Illustration of azimuth, elevation, and deviation angles

B. Communication Model

Due to the absence of physical obstructions, the inter-UAV links are modeled as line of sight (LOS) conditions. Accordingly, the communication channel is modeled using Rician fading with LOS dominance [10]. For a link $i \rightarrow j$, the path loss ($PL_{i,j}$) and the instantaneous received power ($P_{rx_{i,j}}$) are determined as follows:

$$PL_{i,j} = \left(\frac{4\pi \cdot d_{i,j} \cdot f_c}{c}\right)^2 \tag{1}$$

$$P_{rx_{i,j}} = \frac{P_{tx_i} \cdot g_{tx,i} \cdot g_{rx,j} \cdot |h_{i,j}|^2}{PL_{i,j}} \tag{2}$$

where $|h_{i,j}|^2$ represents the power gain of the Rician fading channel. The fading characteristic is defined by the K-factor, which represents the ratio between the power of the LOS component and the scattered multi-path components. In this study, we assume a highly dominant LOS path with $K = 15$ dB [11].

In these expressions, $d_{i,j}$ represents the distance between the two UAVs, f_c is the operating frequency, and c is the speed of light. P_{tx_i} denotes the transmission power, while g_{tx} and g_{rx} represent the linear transmit and receive antenna gains, respectively. To determine the directional antenna gain in dB (G_{tx} and G_{rx}), we employ the 3GPP radiation pattern for directional antennas operating above 6 GHz, which incorporates both horizontal (A_H) and vertical (A_V) components [12]. G_{tx} is formulated as:

$$A_H(\theta_{tx,rx}) = \min\left\{12\left(\frac{\Delta\theta_{tx,rx}}{\theta_{3dB}}\right)^2, A_m\right\}, \tag{3}$$

$$A_V(\phi_{tx,rx}) = \min\left\{12\left(\frac{\Delta\phi_{tx,rx}}{\phi_{3dB}}\right)^2, A_m\right\}, \tag{4}$$

$$G_{tx} = G_{\max} - (A_H(\theta_{tx,rx}) + A_V(\phi_{tx,rx})), \tag{5}$$

where A_m is the sidelobe attenuation, θ_{3dB} and ϕ_{3dB} is the horizontal and vertical 3dB beamwidths and $G_{\max}$ is the peak gain in dB. G_{rx} is also calculated from the receiver antenna's perspective via Equation (5). In our simulations, we assume that a node transmitting to a given receiver does not simultaneously interfere with other receptions at that same receiver UAV.

Using the criteria defined in Equations (3) to (5), the SINR for a link $i \to j$ is now dependent on the spatial filtering of both the transmitter and the receiver. It is expressed as:

$$SINR_{i,j} = \frac{P_{rx,(i,j)}}{N + \sum_{e_{k,g} \in \mathcal{E} \;\; k \notin i,j \;\; g \neq j} I_{k,g \to i,j}} \tag{6}$$

We define $I_{k,g \to i,j}$ as the interference power that the transmission from node k toward node g produces at receiver j while j receives from node i:

$$I_{k,g \to i,j} = \frac{p_{tx_k} \cdot g_{tx,k}(k,g,j) \cdot g_{rx,j}(i,j,k)}{PL_{k,j}} \tag{7}$$

$g_{tx,k}(\cdot)$ is the antenna gain of the interfering transmitter k in the direction of the victim j, relative to its boresight pointing toward g. $g_{rx,j}(\cdot)$ is the antenna gain of the victim receiver j in the direction of the interferer k, relative to its boresight pointing toward its intended transmitter i. Both $g_{tx,k}(\cdot)$ and $g_{rx,j}(\cdot)$ are calculated with Equations (3) to (5).

IV. Problem Formulation and Implemented Algorithms

In multi-hop wireless routing, the maximum achievable end-to-end data rate of a continuous path $\mathcal{P}$ is fundamentally restricted by its weakest link [13]. Our primary objective is to maximize the bottleneck link SINR, which, along with bandwidth, is the main determinant of link capacity. Increasing the capacity of the bottleneck link ensures communication fairness between UAV transmission pairs. In addition to the primary objective, this optimization problem is defined with the following constraints:

- **Strongly Connected Network:** There must be an E2E path exists between any arbitrary pair of nodes.
- **Node Degree:** Each UAV is subject to a degree constraint ($d_{min} \leq d_i \leq d_{max}$), to ensure both path redundancy and hardware feasibility.
- **Bi-directionality:** All established communication links must be bi-directional.

A. Problem Formulation

We formulate a mathematical model to determine the optimal assignment of bidirectional links using directional antennas. The model components—sets, indices, decision variables, and parameters—are defined as follows:

Sets and Indices

- $V = \{1, \ldots, n\}$ represents the UAV set
- $D = \{(i,j) \in V \times V : i \neq j\}$ represents the transmission node pairs
- $T = \{0, \ldots, H-1\}$ represents the considered time window with the steps of 1 second.
- $\mathcal{T}_{\text{quad}} = \{(k,g,i,j) \in V^4 : (k,g) \in D,\ (i,j) \in D,\ k \notin \{i,j\},\ g \neq j\}$ represents the interference quadruples, denoting the interference from link $k \to g$ onto the receiver j, which is oriented towards i.
- $\mathcal{T}_{\text{tri}} = \{(k,g,j) \in V^3 : \exists\, i \in V \text{ s.t. } (k,g,i,j) \in \mathcal{T}_{\text{quad}}\}$ represents the unique interference triples used to define the topological state of the interfering transmitter.
- $r \in V$ represents the root node, which will be used to realize the strongly connected constraint via network flows. It is only an arbitrary node used for the strongly connected constraint.

Decision Variables

- $y_{ij} \in \{0,1\}, \forall (i,j) \in D$: Decision variable for the link $i \to j$ to be active or inactive.
- $f_{ij} \geq 0, \forall (i,j) \in D$: Flow variable used for the strongly connected graph constraint.
- $w_{k,g,j} \in \{0,1\}$: binary indicator equal to 1 if transmission $k \to g$ can interfere with receiver j.
- $\tau \geq 0$: SINR threshold in linear scale.

Parameters

- $S_{i,j,t}$: Received signal power of link $i \to j$ at time t.
- $I_{k,g,i,j,t}$: Interference power received at link $i \to j$ from transmission $k \to g$ at time t.
- N: Noise power.
- d_{min}, d_{max}: Minimum and maximum node degrees.
- M: A sufficiently large constant (Big-M) used to relax the SINR constraint for inactive links.

$$\underset{y,f,w,\tau}{\text{maximize}} \quad \tau$$

subject to

(C-1) $y_{ij} = y_{ji}, \quad \forall (i,j) \in D$

(C-2) $d_{min} \leq \sum_{j \in V \setminus \{i\}} y_{ij} \leq d_{max}, \quad \forall i \in V$

(C-3) $f_{ij} \leq (n-1) y_{ij}, \quad \forall (i,j) \in D$

(C-4) $\sum_{j \in V \setminus \{r\}} f_{rj} - \sum_{j \in V \setminus \{r\}} f_{jr} = n-1$

(C-5) $\sum_{j \in V \setminus \{i\}} f_{ij} - \sum_{j \in V \setminus \{i\}} f_{ji} = -1, \quad \forall i \in V \setminus \{r\}$

(C-6a) $w_{k,g,j} \leq y_{k,g}, \quad \forall (k,g,j) \in \mathcal{T}_{tri}$

(C-6b) $w_{k,g,j} \leq 1 - y_{k,j}, \quad \forall (k,g,j) \in \mathcal{T}_{tri}$

(C-6c) $w_{k,g,j} \geq y_{k,g} - y_{k,j}, \quad \forall (k,g,j) \in \mathcal{T}_{tri}$

(C-7) $\frac{1}{|T|} \sum_{t \in T} \left(\frac{S_{ij,t}}{N + \sum_{(k,g,i,j) \in \mathcal{T}_{quad}} (I_{k,g,i,j,t} \cdot w_{k,g,j})} \right) \geq \ldots$
$\tau - M(1 - y_{ij}), \forall (i,j) \in D$

The primary objective is the maximization of τ. The formula is subject to constraints as:

- (C-1) Bi-directionality.
- (C-2) Node Degree Constraint.
- (C-3), (C-4) and (C-5) are for the strongly connected constraint. It ensures that there is a flow from a root node to any other node in the network.
- (C6a), (C6b), and (C6c) realize the interference rule.
- (C7) Enforces that for every active link, the Arithmetic Mean of the SINR calculated over the time horizon T must be at least τ.

Due to the presence of decision variables in the denominator of C7, the problem is a MINLP. Since MINLP problems are generally NP-hard, we convert it into a MILP as minimizing the maximum Inverse Signal-to-Interference-plus-Noise Ratio (ISINR). The transformations and new parameters are detailed below:

In the original formulation, we defined τ as a variable to serve as a lower bound for all link SINRs. To transform the problem into a minimization of maximum ISINR format, we introduce a new variable, μ, representing the upper bound ISINR across the network. Our reformulated objective is to minimize μ.

For the ISINR definition over a time horizon, we define two new time-averaged parameters, calculated as follows:

- C_{ij}^{base}: The noise-to-signal ratio for link $i \to j$.

$$C_{ij}^{\text{base}} = \frac{1}{|T|} \sum_{t \in T} \frac{N}{S_{ij,t}}, \quad \forall (i,j) \in D \tag{8}$$

- $C_{k,g,i,j}^{\text{int}}$: The ratio of interference power originating from link $k \to g$ to the signal power of link $i \to j$.

$$C_{k,g,i,j}^{\text{int}} = \frac{1}{|T|} \sum_{t \in T} \frac{I_{k,g,i,j,t}}{S_{ij,t}}, \quad \forall (k,g,j,i) \in \mathcal{T}_{quad}, (i,j) \in D \tag{9}$$

With the new parameters, C7 has been transformed in a way to ISINR of every link should be lower than μ. Our new optimization algorithm is as follows:

$$\begin{aligned} &\underset{y,f,w,\mu}{\text{minimize}} \quad \mu \\ &\text{subject to} \\ &\text{Constraints C1 to C6 remain the same} \\ &\textbf{(C-7)} \quad C_{ij}^{\text{base}} + \sum_{\substack{(k,g,i,j) \\ \in \mathcal{T}_{\text{quad}}}} \left(C_{k,g,i,j}^{\text{int}} \cdot w_{k,g,j} \right) \\ &\qquad \leq \mu + M_{ij}(1 - y_{ij}), \quad \forall (i,j) \in D \end{aligned} \tag{10}$$

The Big-M constant in Equation (10) is not chosen heuristically. For each link, we set M_{ij}, which is the largest possible value of the left-hand side of C7, obtained when every candidate interferer is active as below:

$$M_{ij} = C_{ij}^{\text{base}} + \sum_{(k,g):(k,g,i,j) \in \mathcal{T}_{quad}} C_{k,g,i,j}^{\text{int}} - \min_{u,v} C_{uv}^{\text{base}} \tag{11}$$

While the MILP formulation provides an optimal solution, its computational complexity grows exponentially with the number of UAVs. To address this, we have implemented metaheuristic algorithms: GA and GWO.

B. Genetic Algorithm

GA is a stochastic, population-based metaheuristic algorithm. It is widely applied to discrete and combinatorial optimization problems. In GA context, a population of chromosomes evolves over multiple generations in order to find an optimal chromosome, which consists of a gene set, with the best fitness score. Evolution operators in each generation are *selection*, *crossover*, and *mutation*.

C. Grey Wolf Optimizer

GWO is inspired by the leadership hierarchy and hunting mechanism of grey wolves in nature. In the GWO context, the population of candidate solutions has three best solutions, which are the leaders of the population: *alpha* (α), *beta* (β), and *delta* (δ). The top three wolves lead the population toward the optimal solution. Each wolf in the population updates its position based on the mean distance to the leaders, thereby balancing *exploration* and *exploitation* towards the sub-optimal solution.

The correspondence between the network components in the metaphor of metaheuristic algorithms is shown in Section IV-C.

TABLE I: Metaphor Mapping

UAV Network Component	GWO	GA
Network Topology	Wolf Position	Chromosome
Link Status	Position	Gene
Min-SINR Performance	Fitness Score	Fitness Score
Best Global Config.	Alpha (α)	Elite Individual
Configuration Change	Hunting	Mutation/Crossover
Search Direction	α, β, δ guidance	Recombination

Metaheuristic algorithms evaluate the quality of a solution based on its fitness. In our use case, fitness is the mean SINR of the bottleneck link over the time horizon, and the penalties result from the strongly connected and node-degree constraints as in below:

$$P_{deg}(n) = \begin{cases} -(d_{min} - d_n) \cdot 10, & \text{if } d_n < d_{min} \\ -(d_n - d_{max}) \cdot 10, & \text{if } d_n > d_{max} \\ 0, & \text{otherwise} \end{cases} \tag{12}$$

$$F(\mathbf{x}) = \begin{cases} \sum_{n \in \mathcal{V}} P_{deg}(n) + \min_{e \in E} \left(\frac{1}{|\mathcal{T}|} \sum_{t \in \mathcal{T}} \text{SINR}_e(t) \right), & \text{if Connected} \\ -100, & \text{otherwise} \end{cases} \tag{13}$$

In addition to metaheuristic approaches, we implemented the Degree-Constrained Minimum Spanning Tree (DCMST). The DCMST serves two primary functions: providing a performance baseline and initial solution for the metaheuristic algorithms. Unlike purely random initialization, a subset of the initial population—specifically the 'alpha' agent in GWO

or the first chromosome in GA—is seeded with the DCMST result. To explore the neighborhood of this heuristic solution, additional 'seed mutations' are generated by perturbing the seed solution at a predefined rate.

To prevent early convergence to local optima, we implement a reinitialization strategy that reseeds the population if the bottleneck SINR does not improve for a set number of generations. Furthermore, the optimization process terminates if no improvement is recorded over a consecutive number of iterations, defined by the early stop rule. These hyperparameters, summarized in Table II, were calibrated to balance solution quality with computational efficiency.

The population size N_p is dynamically scaled according to the problem dimension D (the number of possible edges) using a population size factor k_{psf}:

$$N_p = \lceil k_{psf} \cdot \sqrt{D} \rceil \tag{14}$$

TABLE II: Metaheuristic Algorithms Parameters

Parameter	GWO	GA
Population Size Factor	4	4
Crossover Rate	-	0.80
Mutation Rate	-	0.02
Elitism Count	2	2
Seed Mutations	5	5
Seed Rate	0.05	0.05
Reinitialization Limit	15	15
Reseed Mutation Rate	0.20	0.20
Early Stop Rule (Generations)	45	45

V. Methodology and Dataset Creation

To address the absence of publicly available multi-hop UAV network datasets, we developed a custom Python-based simulation framework. Node mobility is governed by a three-dimensional Gauss-Markov mobility model to precisely capture temporally correlated flight trajectories. Simulation scenarios explicitly target high-mobility regimes, with mean node velocities ranging from $100\,\mathrm{m/s}$ to $200\,\mathrm{m/s}$.

The candidate algorithms are evaluated across 170 distinct network instances containing 10–50 nodes. To systematically assess physical-layer robustness, each network instance is tested under multiple configurations by varying the transmit power (P_{tx}), antenna beamwidth (θ_{3dB}), and the minimum node degree constraint (d_{min}). Executing each candidate algorithm across the full combination of 170 instances and 9 parameter sets yields a comprehensive evaluation pool of $1,530$ unique topology realizations.

To enhance the practical relevance of our evaluation, we include antenna pointing errors. The angular jitter in both azimuth and elevation is modeled as an independent Gaussian process, $\mathcal{N}(0, \sigma^2)$, with a standard deviation of $\sigma = 1^\circ$ [14]. Once the network topologies are established by the respective algorithms, their performance is evaluated over 1,000 Monte Carlo iterations to account for stochastic fading and misalignment effects. Results are assessed and compared using mean values and Cumulative Distribution Functions (CDFs).

TABLE III: Communication Parameters for 5G URLLC Simulation

Parameter	Value
Minimum number of the connections (d_{min})	$(1, 2, 3)$
Maximum number of the connections (d_{max})	4
Maximum Antenna Gain (G_{max})	20 dB
Side Lobe Attenuation (A_m)	30 dB
Antenna Beamwidth (θ_{3dB}, ϕ_{3dB})	$\{15^\circ, 30^\circ, 45^\circ\}$
Rician K-factor	15 dB
Transmit Power (P_{tx})	$\{14, 17, 20\}$ dBm
Channel Bandwidth (BW)	100 MHz
Carrier Frequency (f_c)	31 GHz
Subcarrier Spacing (Δf)	120 kHz
Number of Resource Blocks (N_{PRB})	66
Symbol Duration (T_s)	8.93 μs
Scaling Factor (f)	0.8
Overhead Percentage (OH)	0.2
MIMO Layers (v_{Layers})	1
Target BLER	10^{-8}

We evaluate the impact of maximizing the minimum SINR by focusing on the link data rate, as the bottleneck link fundamentally constrains the maximum achievable E2E capacity [13]. Accordingly, we measure network effectiveness through the mean E2E capacities across all transmission pairs. To assess the equitable distribution of these data rates across the swarm, we apply Jain's Fairness Index [15]. For n active links with data rates $R = \{R_1, R_2, \ldots, R_n\}$, Jain's Fairness Index is defined as:

$$\mathcal{J}(R) = \frac{\left(\sum_{i=1}^{n} R_i\right)^2}{n \cdot \sum_{i=1}^{n} R_i^2} \tag{15}$$

The link data rate is derived using a two-stage link adaptation procedure. First, the instantaneous SINR is mapped to a Modulation and Coding Scheme (MCS) based on the study in [16]. The MCS is selected with the alignment of Ultra-Reliable Low-Latency Communications (URLLC), such that the Block Error Rate (BLER) is maintained at 10^{-8}. Second, the physical layer data rate, R, is calculated according to the 3GPP TS 38.306 standard [17] using the following formulation:

$$R = v_{Layers} \cdot Q_m \cdot f \cdot R_{code} \cdot \frac{N_{PRB} \cdot 12}{T_s} \cdot (1 - OH) \tag{16}$$

where v_{Layers} is the number of MIMO layers, Q_m is the modulation order, f is the scaling factor, R_{code} is the code rate of the selected MCS, N_{PRB} is the number of allocated resource blocks, OH is the signaling overhead, and T_s is the average OFDM symbol duration. The communication parameters utilized in this simulation are summarized in Table III.

All simulations and optimizations were conducted on a Dell Latitude 5440, equipped with an Intel Core i7 processor. The simulation environment, MILP, and metaheuristic algorithms were implemented in Python. The MILP model was solved using the SCIP Optimization Suite [18].

TABLE IV: Mean Performance Metrics Across All Evaluated Network Instances

Algorithm	Min SINR	Min Rate	Avg E2E Capacity	Fairness
	(dB)	(Mbps)	(Mbps)	(Jain's)
DCMST	-6.132	5.828	35.738	0.211
GA	-1.577	19.719	37.967	0.215
GWO	-1.468	20.272	29.772	0.167
MILP	0.395	30.058	47.264	0.274

VI. Results and Discussion

This section evaluates the performance of the proposed algorithms. While the evaluation considers a 60-second time horizon, this parameter remains adjustable to suit various operational scenarios. Performance is assessed based on three primary metrics: the bottleneck link data rate, the average E2E capacity across all feasible flows, and the total computation time. We present bottleneck link SINR results exclusively in Table IV and Figure 3a; for the remaining analyses, this metric is omitted. The main reason behind that SINR and link data rate are directly proportional, as the latter is derived through the SINR-to-MCS mapping detailed in Section V. Our primary objective is to maximize the minimum SINR, thereby enhancing the bottleneck data rate and promoting network fairness. Finally, we characterize overall network performance by examining the average E2E capacity across all possible transmission pairs.

Table IV summarizes the results by averaging the considered metrics across all optimized network instances. As expected, MILP achieves the highest performance metrics and serves as the benchmark. Conversely, DCMST exhibits the lowest performance because it optimizes solely for distance, without accounting for interference. As shown by the average E2E capacity and minimum link data rate metrics, these metrics exhibit a trend similar to the minimum SINR. It confirms that maximizing the quality of the bottleneck link enhances the broader E2E network performance. On the other hand, Jain's index shows that we can improve network fairness by maximizing the minimum link data rate.

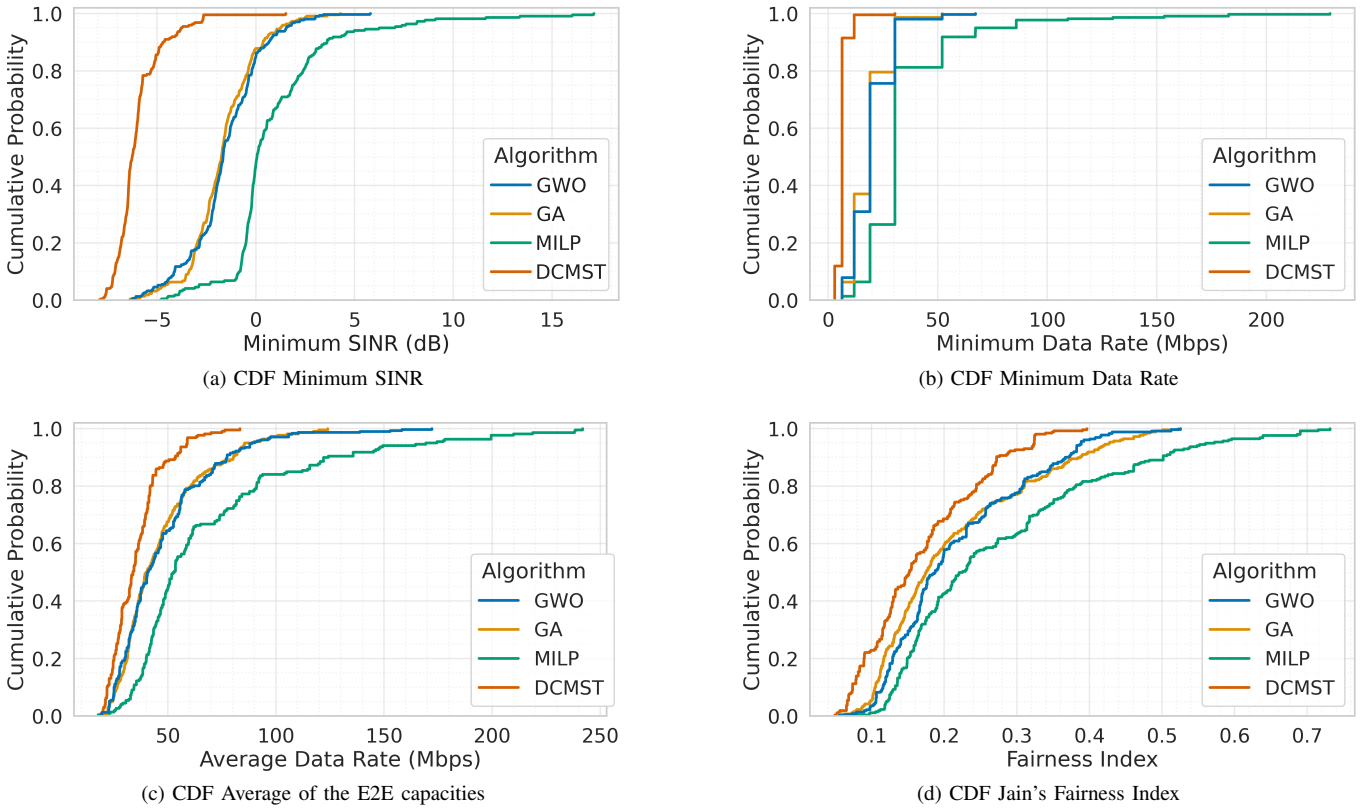
Figure 2 illustrates the CDF for the minimum SINR, bottleneck data rate, and average E2E capacity. These results characterize the robustness of the algorithms under stochastic channel impairments, specifically Gaussian-distributed misalignment and Rician fading. As shown in Figure 2a, the MILP formulation exhibits clear dominance, shifting significantly to the right with a gain of approximately 2 dB and 7 dB over the metaheuristic and heuristic approaches, respectively. While the metaheuristic variants perform similarly, the heuristic baseline consistently yields the lowest SINR distribution.

As illustrated in Figure 2b, the bottleneck link data rate follows a similar trajectory but exhibits pronounced stepwise behavior. This pattern arises from the discrete MCS mapping, in which data rate improvements occur only when the SINR crosses specific quantization thresholds. Furthermore, Figure 2c evaluates the average E2E capacity across all network flows. Although the performance gap between algorithms narrows when considering aggregate metrics, the performance order remains consistent. This convergence is unsurprising, as the optimization focus is on maximizing bottlenecks rather than enhancing the global average. Finally, Figure 2d depicts the CDF of Jain's fairness index. While the trends mirror those of the average capacity, the performance disparities between the algorithms are more pronounced, indicating significant differences in how equitably each method distributes network resources.

Figure 3a illustrates the bottleneck link data rate as a function of network size. The MILP formulation consistently achieves the highest performance, representing the global optimum for each scenario. In contrast, the metaheuristic algorithms provide sub-optimal solutions that do not strictly dominate one another across varying network scales. Notably, as node density increases, the performance of metaheuristics tends to plateau because these algorithms become trapped in local optima as the search space expands. Conversely, the MILP effectively leverages the additional topological opportunities provided by additional nodes to identify superior topologies, leading to a marked increase in the minimum data rate.

The evaluation of average E2E capacity relative to network size is illustrated in Figure 3b. A key observation is that the performance disparity between the MILP, metaheuristic, and DCMST approaches increases as the network expands. While the differences remain marginal for smaller configurations (15–25 nodes), the advantage of sophisticated optimization becomes significantly more pronounced in larger networks. This suggests that maximizing the bottleneck link data rate is a more effective strategy for enhancing global network performance as network size increases. Finally, we analyze network fairness as a function of network size in Figure 3c. Fairness follows a trend similar to the average E2E capacity, performance beginning to diverge notably beyond the 25-node threshold. This divergence indicates that in larger networks, optimized algorithms are better equipped to distribute interference-induced degradation equally across the network. By preventing interference from clustering on specific links, these algorithms maintain a more uniform distribution of data rates across all transmission pairs.

The impacts of key parameters on the bottleneck link data rate, average E2E capacity, and network fairness are summarized in Figure 4. Specifically, Figure 4a and Figure 4b highlight a strong negative correlation between antenna beamwidth and overall performance: wider beams degrade spatial filtering, increasing inter-link interference and reducing network-wide SINR. This degradation directly limits the bottleneck link data rate. Notably, this impact is more pronounced for average E2E capacity than for the bottleneck metric, as E2E capacity accumulates interference across all links along a multi-hop path rather than on a single constraining link. Mirroring these throughput metrics, Jain's fairness index also declines as beamwidth increases. Although relative algorithm rankings remain stable across beamwidths, the performance gap between approaches narrows in high-interference regimes; specifically, the competitive advantage of MILP over metaheuristics—and



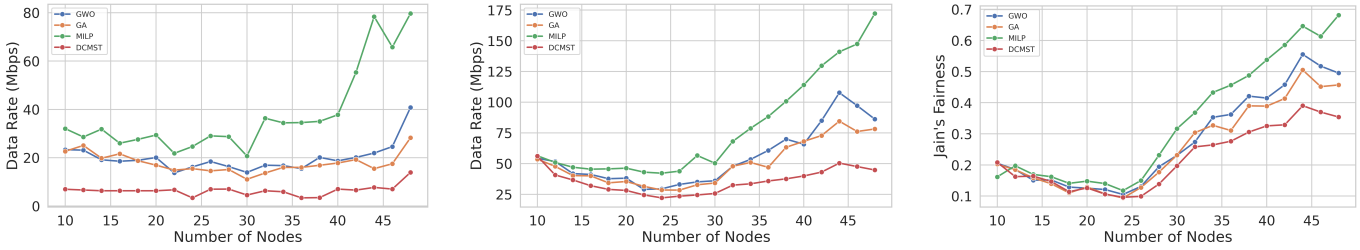
(a) CDF Minimum SINR

(b) CDF Minimum Data Rate

(c) CDF Average of the E2E capacities

(d) CDF Jain's Fairness Index

Fig. 2: CDF of the metrics over the Monte Carlo Simulations



(a) Bottleneck Link Data Rate

(b) Average E2E Capacity

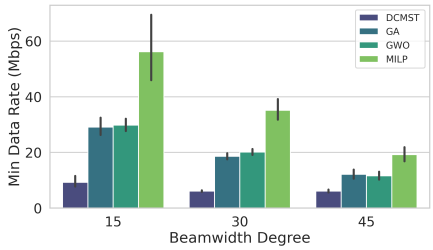
(c) Jain's Fairness Index

Fig. 3: The impact of network size on the bottleneck link data rate, average E2E capacity, and network fairness.

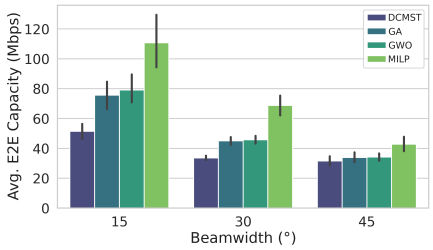
of metaheuristics over the baseline DCMST—diminishes as wider beams become the dominant performance bottleneck.

Compared to antenna beamwidth, transmit power has a significantly weaker influence on both the bottleneck link data rate and average E2E capacity. Throughput exhibits only marginal gains as transmit power increases, confirming that the network operates in an interference-limited regime where aggregate interference scales proportionally with signal power. Consequently, as illustrated in Figure 4d, elevated signal power is insufficient to overcome interference at the bottleneck link. Although Figure 4e shows a slightly larger improvement in average E2E capacity, overall gains remain negligible. The most pronounced impact of transmit power is on the fairness index, which degrades as transmit power increases. This widening throughput disparity occurs because low-interference links capture most of the power gain, whereas high-interference links experience an elevated interference floor that neutralizes or reduces their SINR. Unlike varying beamwidth, adjustments to transmit power preserve both relative algorithm rankings and performance gaps.

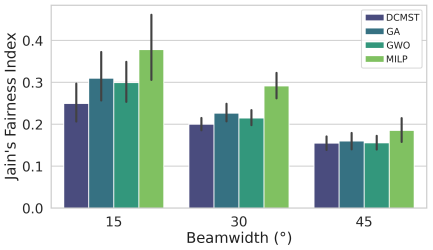
The final parameter evaluated is the minimum connectivity constraint (d_{min}). As illustrated in Figure 4g and Figure 4h, both bottleneck data rate and average E2E capacity are inversely proportional to d_{min}. Stricter connectivity constraints force higher network density, increasing interference and degrading link data rates. Notably, as d_{min} scales, the performance gap between algorithms narrows, diminishing the advantages of the MILP and metaheuristics over DCMST. This



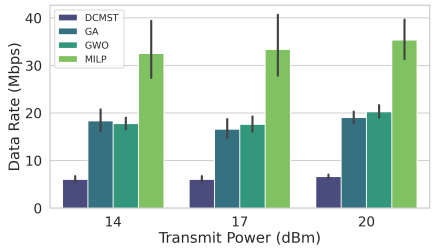
(a) Beamwidth Degree Impact on Bottleneck Link



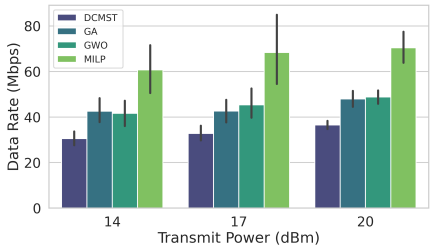
(b) Beamwidth Degree Impact on Average E2E capacity



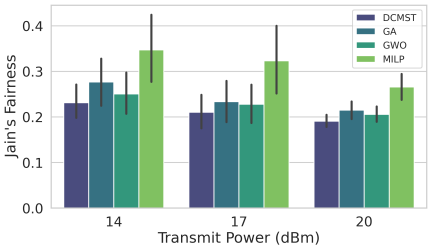
(c) Beamwidth Degree Impact on Fairness



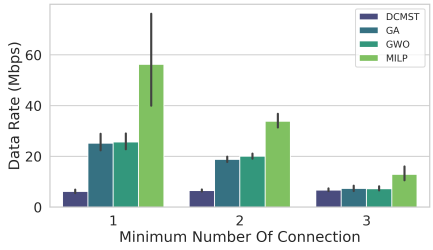
(d) Transmit Power Impact on Bottleneck Link



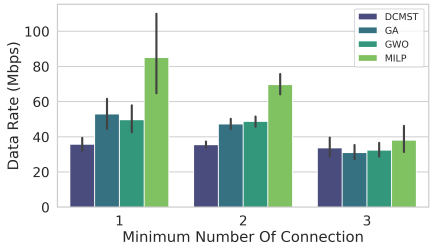
(e) Transmit Power Impact on Average E2E capacity



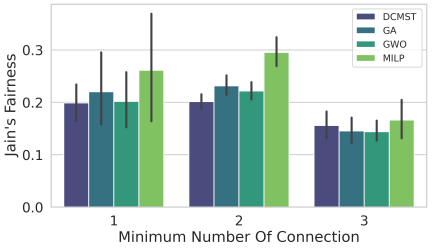
(f) Transmit Power Impact on Fairness



(g) Min Connection Constraint Impact on Bottleneck Link



(h) Min Connection Constraint Impact on Average E2E capacity



(i) Min Connection Constraint Impact on Fairness

Fig. 4: The impact of network parameters on the bottleneck link data rate, average E2E capacity, and network fairness. The bars represent the mean values of the simulations, and the error lines denote the 95% confidence intervals.

introduces a critical trade-off: higher connectivity improves robustness but directly penalizes bottleneck throughput. As shown in Figure 4i, the lowest fairness levels are recorded at $d_{min} = 3$. This is attributed to the high variance in individual link capacities at this degree; while some links maintain high data rates, the bottleneck links are significantly constrained, leading to a wider performance disparity. Lastly, MILP results at lower connectivity exhibit wider confidence intervals due to a broader distribution of possible topological outcomes than in denser configurations.

Figure 5 illustrates algorithm execution times across network sizes on a logarithmic scale. The heuristic-based DCMST achieves the lowest execution time. While MILP is efficient for small networks—outperforming some alternatives at up to 14 nodes—its computational requirements grow exponentially, rendering it infeasible for larger scales. Among metaheuristics, GWO proves computationally more efficient than GA. Operationally, neither MILP nor metaheuristic frameworks support real-time execution. However, minimized computation time is vital for emergency response planning where rapid deployment is critical. For larger topologies, metaheuristic algorithms offer a highly practical alternative due to their significantly reduced planning time.

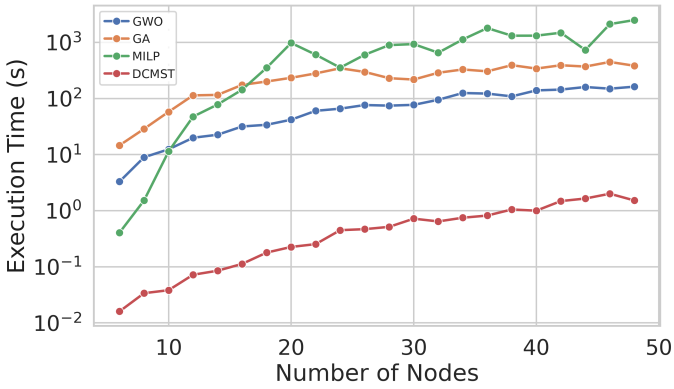


Fig. 5: Computation Time vs Number of Nodes

VII. Conclusion and Future Work

This study investigated topology optimization in UAV Ad-Hoc networks by maximizing the bottleneck SINR using MILP, GWO, and GA. We first formulated the optimization as a MINLP problem under specific network constraints, which was subsequently linearized into a MILP formulation for solution via an exact solver. To achieve high-quality solutions within practical time limits, we implemented metaheuristic algorithms—specifically GA and GWO—alongside a DCMST-based heuristic.

The performance of these algorithms was evaluated under stochastic conditions, including Rician fading channels and antenna misalignment, across various parameter sets, including transmit power, beamwidth, and connectivity requirements. By analyzing metrics including the bottleneck link data rate, average E2E capacity, and network fairness, we characterized the performance trade-offs inherent in UAV swarms. Our results demonstrate that while MILP provides the theoretical upper bound for network performance, metaheuristic approaches yield viable suboptimal solutions with significantly reduced computational overhead. This analysis clarifies which algorithm and parameter set is more suitable for which network size and parameter set.

Our approach is applicable to various UAV swarm missions that rely on offline planning with dynamically evolving trajectories. Because these pre-planned paths shift during execution, the network topology must be recomputed at each time horizon H and remain fixed during that horizon to prevent resynchronization and overhead. Example use cases include agricultural surveying, environmental mapping, and general monitoring.

While this work establishes a robust optimization framework, it also leaves room for future research. Future extensions could consider scenarios for space- air- ground integrated networks. Additionally, the implementation of machine learning-based algorithms, such as reinforcement learning, could offer significant potential to further reduce computation time while delivering high-quality solutions, making them ideal for deployment.

References

[1] H. Shakhatreh, A. H. Sawalmeh, A. Al-Fuqaha, Z. Dou, E. Almaita, I. Khalil, N. S. Othman, A. Khreishah, and M. Guizani, "Unmanned aerial vehicles (uavs): A survey on civil applications and key research challenges," *IEEE access*, vol. 7, pp. 48 572–48 634, 2019.

[2] W. Zhang, W. Zhang, and J. Wu, "Uav beam alignment for highly mobile millimeter wave communications," *IEEE Transactions on Vehicular Technology*, vol. 69, no. 8, pp. 8577–8585, 2020.

[3] J. H. Holland, *Adaptation in Natural and Artificial Systems: An Introductory Analysis with Applications to Biology, Control, and Artificial Intelligence*. Ann Arbor, MI: University of Michigan Press, 1975.

[4] S. Mirjalili, S. M. Mirjalili, and A. Lewis, "Grey wolf optimizer," *Advances in engineering software*, vol. 69, pp. 46–61, 2014.

[5] R. Ramanathan and R. Rosales-Hain, "Topology control of multihop wireless networks using transmit power adjustment," in *Proceedings IEEE INFOCOM 2000. Conference on Computer Communications. Nineteenth Annual Joint Conference of the IEEE Computer and Communications Societies (Cat. No. 00CH37064)*, vol. 2. IEEE, 2000, pp. 404–413.

[6] S. Hofmann, V. Megas, M. Ozger, D. Schupke, F. H. Fitzek, and C. Cavdar, "Combined optimal topology formation and rate allocation for aircraft to aircraft communications," in *ICC 2019-2019 IEEE International Conference on Communications (ICC)*. IEEE, 2019, pp. 1–6.

[7] V. Megas, S. Hoppe, M. Ozger, D. Schupke, and C. Cavdar, "A combined topology formation and rate allocation algorithm for aeronautical ad hoc networks," *IEEE Transactions on Mobile Computing*, vol. 23, no. 1, pp. 12–28, 2022.

[8] B. Newton, J. Aikat, and K. Jeffay, "Explicit topology management for continental-scale airborne networks," in *2017 IEEE Conference on Computer Communications Workshops (INFOCOM WKSHPS)*. IEEE, 2017, pp. 72–77.

[9] H. Wang, B. Jiang, H. Zhao, J. Zhang, L. Zhou, D. Ma, J. Wei, and V. C. Leung, "Joint resource allocation on slot, space and power towards concurrent transmissions in uav ad hoc networks," *IEEE Transactions on Wireless Communications*, vol. 21, no. 10, pp. 8698–8712, 2022.

[10] E. Haas, "Aeronautical channel modeling," *IEEE transactions on vehicular technology*, vol. 51, no. 2, pp. 254–264, 2002.

[11] X. Cao, P. Yang, M. Alzenad, X. Xi, D. Wu, and H. Yanikomeroglu, "Airborne communication networks: A survey," *IEEE Journal on Selected Areas in Communications*, vol. 36, no. 9, pp. 1907–1926, 2018.

[12] 3rd Generation Partnership Project (3GPP), "Study on channel model for frequency spectrum above 6 GHz," 3GPP Technical Specification Group Radio Access Network, Technical Report (TR) 38.900, 6 2018.

[13] K. Jain, J. Padhye, V. N. Padmanabhan, and L. Qiu, "Impact of interference on multi-hop wireless network capacity," in *Proceedings of the 9th annual international conference on Mobile computing and networking*, 2003, pp. 60–73.

[14] M. T. Dabiri and M. Hasna, "Pointing error modeling of mmwave to thz high-directional antenna arrays," *IEEE Wireless Communications Letters*, vol. 11, no. 11, pp. 2435–2439, 2022.

[15] R. K. Jain, D.-M. W. Chiu, W. R. Hawe *et al.*, "A quantitative measure of fairness and discrimination," *Eastern Research Laboratory, Digital Equipment Corporation, Hudson, MA*, vol. 21, no. 1, pp. 2022–2023, 1984.

[16] L. Li, Q. Jiang, and W. Luo, "A unified non-cqi-based amc scheme for 5g nr downlink and uplink transmissions," in *2021 IEEE 6th International Conference on Computer and Communication Systems (ICCCS)*. IEEE, 2021, pp. 881–886.

[17] 3rd Generation Partnership Project (3GPP), "Technical Specification Group Radio Access Network; NR; User Equipment (UE) radio access capabilities (Release 18)," 3GPP, TS 38.306, 2024.

[18] T. Achterberg, "Scip: solving constraint integer programs," *Mathematical Programming Computation*, vol. 1, no. 1, pp. 1–41, Jul 2009. [Online]. Available: https://doi.org/10.1007/s12532-008-0001-1